Ewald Ionic Maps Gauging the Effect of Solvent Interaction on Crystal Morphology Illustrated by Surface X-ray Diffraction of Potassium Dihydrogen Phosphate

C. S. Strom

SeriousToo Crystal Morphology Software, P. O. Box 2139, 1000 CC, Amsterdam, The Netherlands

Received: July 28, 1999

Ewald maps provide an exact assessment of the fine-scale electrostatic behavior of the combined bulk-cell and surface-cell trial solutions used in interpreting X-ray diffraction data on ionic surfaces. Thus, insight can be gained in the effect of the surface electric-field distribution and surface polarity on crystal morphology. A spatial distribution of the solvent- or impurity-accessible surface locations is determined as a function of the van der Waals spheres of the solid and fluid species. The electrostatic potential and electric field vector are computed on the resulting undulated input surface, by means of an analytical formulation of the Ewald method adapted to laminas. Equipotential and equifield contours enable the identification of possible adsorption sites of cations on local potential minima, anions on local potential maxima, and neutral polar particles (e.g., water) on local field maxima. Experimentally observed surface reconstruction can be accounted for by distinguishing between a "surface cell" generating the top (*hkl*) layer adjacent to the liquid and a "bulk cell" generating all subsequent layers. Exactness and model independence avoid fundamental inconsistencies inherent in approximate and intuitive approaches encountered in recent literature. The electric field distribution on the crystal surface determines the effect of a polar liquid on the growth form. General applicability to structures with a dominant ionic character is ensured. An application to potassium dihydrogen phosphate, $K^+H_2PO_4^-$ (KDP), is presented.

1. Introduction

Electrostatic and in particular polarity properties of growing surfaces are crucial in determining the morphology of ionic crystals in regard to the following: energy gain by surface relaxation or reconstruction or by interaction with solvent; dipole-moment neutralizing mechanisms taking place in the absence or presence of impurities; solvation of the surface by polar particles; and ion attachment.

The difference in morphological importance between the pyramid and the prism in the actual growth form of potassium dihydrogen phosphate (KDP), as compared to the basic theoretical growth form, is attributed to the interaction during growth of the KDP surfaces[1,2] with the pure or impure aqueous solution and the role of dehydration. Recently, the surfaces of KDP ($K^+H_2PO_4^-$) were observed by surface X-ray diffraction.[2] Experimental results on the pyramidal growth front were misinterpreted as a result of inadequate theoretical methods for determining growth layer compositions and surface electrostatic quantities.

At present, techniques like surface X-ray diffraction can only deal with uncomplicated fairly planar surface compositions in near-equilibrium conditions. As the experimental capabilities extend beyond simple structures, the need for potent theoretical interpretation becomes accute. Needs for accessing the experimental outcome include the following:

Knowledge and Utilization of All Possible Trial Solutions. When data processing relies on trial-and-error procedures, the complete set of trial solutions[3−5] for the "surface cell" and "bulk cell" should not be restricted a priori and intuitively.

Preventing Loss of Information. It is customary in the context of the Hartman−Perdok theory[6,7] to characterize growth layers by their slice energies or attachment energies, or the interaction energy of a given surface boundary with a single molecule acting as a possible inhibitor. Especially the former practice entails loss of information by reducing the rich complexity of a surface to a single number. Ionic surface maps compensate for that loss.

Exactness in the Case of Dominance by Coulomb Forces. Electrostatic surface properties depend on the entire content of the experimentally obtained surface and bulk cells as well as on the—practically infinite—number of layers contained in the physical specimen used for the experiment. Whereas in cases of dominance by short-range forces the surface and near-surface behavior follows by restricting attention to the surface boundary, in cases of Coulomb dominance that approximation fails as it leads to self-contradictions.

Electric Field Distribution on the Surface. It must enter the picture to account for the action of the near-surface polar liquid, e.g., aqueous solution. Experiments prove[8] that when a given compound grows out of a nonpolar solution, the nonpolar faces dominate, whereas when it grows out of a polar solution, the polar faces dominate; e.g., the interaction of the surface electric field distribution with the adjacent polar water molecules[9] revealed a water layer functioning as an interfacial "skin" on the calcite rhombohedron.

2. Fundamental Inconsistenties in an Intuitive Approach to Surface Electrostatics

The sensitive interdependence between trial solutions of surface configurations and expected electrostatic surface behavior is summarized in the concluding section.

A basic flaw exemplified by the recent interpretation of surface X-ray diffraction results on KDP[2] rests on the assumption that the outermost charge distribution at the surface

10.1021/jp992652j CCC: $18.00
Published on Web 12/07/1999

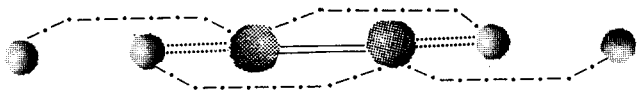

Figure 1. Larger ($H_2PO_4^-$) and smaller (K^+) spheres are ions in the actual growth layer[5,10] of the KDP prism. The direction of view is parallel to the growth layer. Double solid lines, hydrogen bonds; double dotted lines, g-bonds coinciding in projection; dashed-dotted lines, h-bonds.

termination of a growth layer in a crystal is the physical quantity governing the electrostatic behavior and especially polarity of surfaces and interfacial material. In that work the observation of the prismatic and pyramidal surface compositions, shown respectively in Figures 1 and 2A,[10,11] confirms previous theoretical and experimental results (e.g. refs 1 and 12). The outermost pyramidal surface boundary of Figure 2A consisting of a K^+ ion array gave a good fit to the X-ray diffraction data. A better fit[2] was obtained after applying a small amount of surface relaxation.

However, the determination of the layer-generating cell(s) from diffraction data relies solely on a trial-and-error method, whereby the validity of a given solution is assessed by the goodness of its fit. Good fits may emerge from none, one, or more solutions. Although complete sets of trial solutions and their orientations, derived theoretically for KDP by the Hartman−Perdok theory,[3−7] are available in the literature,[1,10] the set of trial solutions employed by ref 2 was unjustifiably restricted on unspecified grounds. Fits corresponding to distinct trial solutions, possessing identical surface boundaries and the same step height (e.g., Figures 2C and 2D) as the configuration finally selected in ref 2 (Figure 2A), were ignored.

In examining the morphological implications for the KDP growth form, the authors in ref 2 (p 2232) characterize the experimentally observed surface shown in Figure 2A as "strongly polarized" and proceed to describe the resulting "intriguing implications for the near-surface liquid". The authors reason that because the half-step-height layer d_{202} (shown in Figure 2B) is strongly polarized, then the full-step-height layer d_{101} (shown in Figure 2A) must also be strongly polarized, on grounds that these d_{101} and d_{202} layers are bounded by identical surface terminations adjacent to the fluid. Noteworthily the d_{101} layer of Figure 2A is associated with the cell observed experimentally in ref 2, while the d_{202} trial solution disagrees with the X-ray data. Moreover, the symmetry point located in the middle of the unrelaxed d_{101} growth layer of Figure 2A results in symmetrically identical oppositely lying surface boundaries. And consequently it forces the surface dipole[13] of Figure 2A to vanish, giving rise to a nonpolar surface. Because surface reconstruction tends to neutralize any existing surface dipole rather than enhance it, it is implausible that the modest effect of a ∼0.1 Å relaxation observed in ref 2 could cause a nonpolar layer to become "strongly polar".

The presumed polarization of the experimentally determined pyramidal surface is erroneously inferred from the outermost charge configuration, that is, a K^+ array at height $^1/_4d$ above an $H_2PO_4^-$ array. It rests on the intuitive but flawed notion that surface polarity could be caused when a plane containing charges of a given sign is followed by a plane containing charges of the opposite sign. Such an assumption is as untenable (at the surface-atomic level a strict geometrical plane is hardly meaningful) as it is self-contradictory. Thus, in the (100) surface layer of KDP in Figure 1, which is correctly considered nonpolar,[2] planes composed of negative atomic charges, e.g., the oxygens of the $H_2PO_4^-$ molecules (included in the large spheres in the figure) follow planes composed of positive K^+ charges (small spheres), even though the molecular mass centers lie on the same plane.

A second inconsistency is related to the a priori restriction of the used set of trial solutions. Growth layers B, C, and D in Figure 2 are examples of the trial solutions (computed graph-theoretically by program FFACE[3−5,10]) that have identical K^+ terminations at the interface (shown by wedged lines in the figure) as the experimentally determined growth layer A. The half-layer B with step height 2.05 Å, and the full layers C and D with the same step height as A, 5.10 Å, are all polar. Layers A, B, C, and D have radically different surface polarities, yet at the interface they have identical terminations, their compositions overlapping by as much as 50%. (For example, the surface dipole of C, −5.32 eÅ, is caused by the simplest form of irreducible borders,[5] that is, dangling bonds, opposite the surface in the direction of the bulk.[14]) If the surface−solvent interaction depended directly on the termination charges,[2] then growth layers such as A, C, and D would trigger identical behavior at the near-surface liquid, implying that crystal growth should result in identical morphology when occurring in polar and nonpolar environments;[15] abundant literature proves the opposite (see ref 8).

The premise "Since crystal growth takes place at the crystal−solution interface, one expects the atomic structure at this boundary to play a primary role ..."[2] is invalid for electrostatic forces. Surface polarity is defined by the surface dipole[13] and depends on the charges within the *entire* experimentally determined cell, generating the observed growth layer; and not just a portion of that cell, generating the termination. The resulting behavior of the polar near-surface liquid is governed by the surface distributions, *not* of the termination charges, but of the electrostatic potential and/or electric field (cf. ref 15) caused by the charge distribution of the *entire* aforementioned layer. The physical crystal sample used for the experiment is approximated by a semi-infinite stacking of these layers.[16,17] Thus, *identical* surface charge terminations generated by *different* cells *can* exhibit *different* surface polarities and consequently *can* and *do* trigger *different* behavior at the near-surface liquid in accord with observation.[8]

3. Surface Maps Constructed from Distributions of Electrostatic Potential and Electric Field

Trial solutions for the bulk and surface cells are employed to fit the experimental points obtained for the (*hkl*) surface. When the bulk and surface cells concide, the attempted fit involves an unreconstructed surface. Possible surface relaxation or reconstruction is reflected in a difference between bulk and surface cells. Rapid convergence ensures that trial solutions for both unreconstructed and reconstructed surfaces can be equally well accommodated in the present maps. A series of ionic surface maps is constructed for each specific value of the van der Waals radius for a given particle species in the interfacial medium.

In the near-surface material cations respond to local minima of the site potential and anions to local maxima. Polar particles like water molecules respond to local maxima of the electric field, tending to align their dipoles with that vector. Solvent and impurity particles adsorb at accessible surface locations, tending to maximize their interaction with the surface.

The site potential and site electric field vector caused by any collection of layers, i.e., laminas, and sampled at any point in space $\vec{R}$[17] are computed by the Ewald method[18] adapted in closed analytical form[16] to two-dimensional cases. A series of ionic surface maps is constructed for each specific value of the van

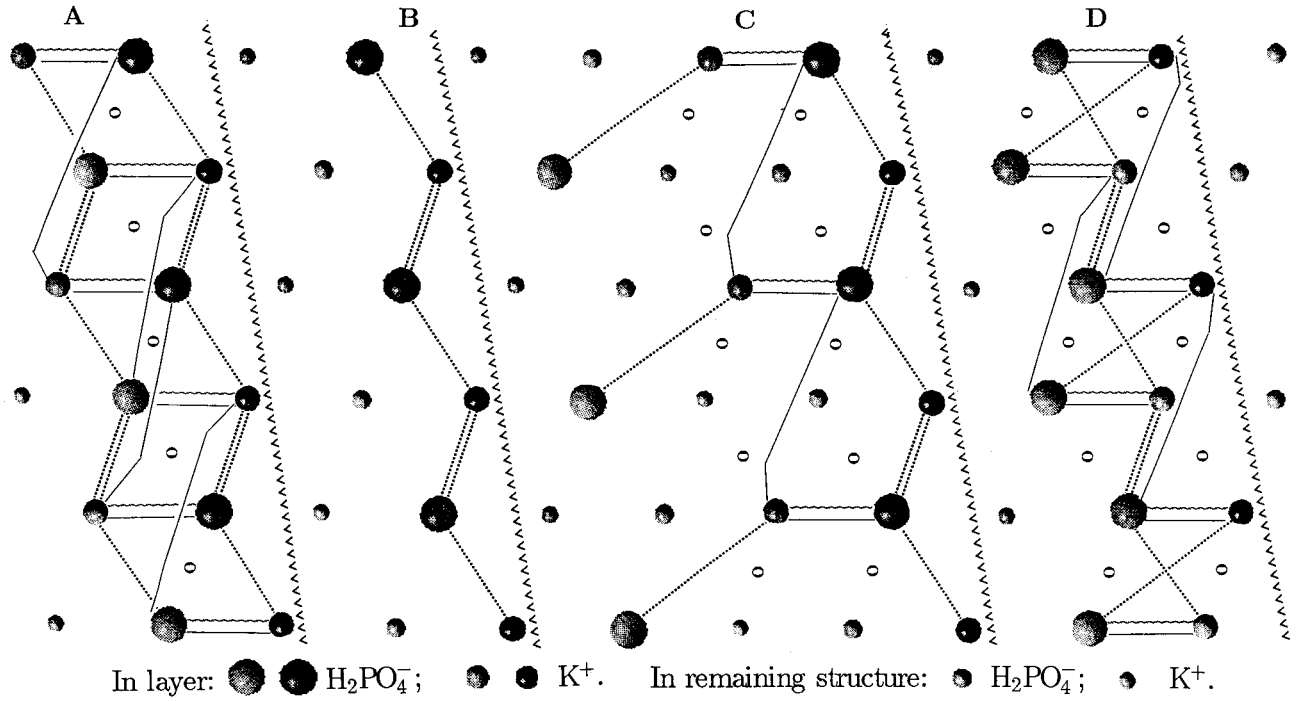

Figure 2. Larger ($H_2PO_4^-$) and smaller (K^+) spheres are ions in some of the theoretical growth layers in the KDP pyramid. Ions in the remaining structure are scaled down. The direction of view is parallel to the growth layers, the growth fronts indicating the crystal−solution interfaces are marked by wedged lines. Black spheres indicate overlapping molecular boundary compositions and surface terminations, that is, portions common to the depicted growth layers adjacent to the solution; gray spheres are the distinct portions of the depicted growth layers on the side of the bulk. Open circles, symmetry centers; wavy lines, f-bonds; dotted lines, g-bonds; solid lines, h-bonds. Hydrogen bonds are not shown. Surface dipoles in eÅ using formal charges: observed layer A, 0; B, −1.33; C and D, −5.32.

der Waals radius for a given particle species in the interfacial medium. The results are exact and independent of any adjustable parameters. The site potential and electric field caused by an infinite stacking of laminas parallel to (*hkl*) is obtained (program SURFPOT[17]), by summing over the layer index, say $m = -1...\infty$. Because of the excellent convergence properties of the Ewald summation, ∞ is adequately replicated by 3−10 laminas or 5−15 Å.

Surface reconstruction can be simulated by taking an artificially long unit cell consisting of a few bulk cells stacked parallel to (*hkl*) with the specified surface cell at the top. An application involving such "sandwich" layers is found in refs 9 and 17. Provided the first artificially long sandwich layer falls within the margin of convergence, that is, as long as convergence is achieved for $m = 1$, the obtained results are equally exact as in the customary semi-infinite stacking of ordinary layers.

The Appendix outlines the construction of an undulated surface of closest approach between the van der Waals spheres of the solid and fluid particles. The spatial distribution of sites on such a surface is used as input for the computation of potential and field (programs SURFPOT and SURFGRID[17,19]). Contour plots follow from the values of these quantities on the grid points of this undulated surface. The surface cell could also be made to include steps and kinks, cf. ref 15, by choosing an appropriate artificially large unit cell on the (*hkl*) face. The adsorption sites of the various chemical species in the near-surface liquid are brought into the picture for a variety of ionic surface configurations.

4. Surface Maps of the KDP Prism

Some illustrations follow for the prismatic growth layer of KDP of Figure 1. No relaxation or reconstruction could be expected in this monomolecular sheet of centrosymmetric molecules and none is observed.[2] The surface maps of Figures 3−5 cover a number of primitive unit cells parallel to the prismatic surface of KDP. They refer to adsorption sites of a fluid particle with a typical VDW radius of 0.8 Å taken to be a cation in Figure 3b, 2.0 Å taken to be an anion in Figure 4b, and 1.4 Å taken to be an anion (on the left side) or a cation (on the right side) of Figure 5b and a water molecule in Figure 5c.

Figures 3a, 4a, and 5a cover 2 × 1 primitive unit cells or ∼7.8 × 3.9 Å and correspond to the upper half portions of Figures 3b, 4b, and 5b,c. They show height contours of the undulated surface of closest approach between the van der Waals spheres of the structure particles and the reference fluid particles. Dashed lines indicate the lowest lying points. These figures are the spatial distributions used as input for the resulting surface maps shown in the remaining figures. Noteworthy is the ribbed or steplike pattern of the prism for all three van der Waals radii, as expected by inspection of Figure 1. Each rib is broad for fluid particles of $r_{VDW} = 0.8$ Å, splits into two thinner and sharper ribs for fluid particles of $r_{VDW} = 1.4$ Å, and rejoins again into a broad shifted rib for fluid particles of $r_{VDW} = 2.0$ Å.

The spatial distributions of Figures 3a and 4a are input for computing the corresponding contours of the electrostatic potential in Figures 3b and 4b. Figure 5a is input for the potential and field contours of Figure 5b,c, respectively. The equipotential maps exhibit patterns analogous to those of the height contours. Solid lines indicate positive, dashed lines negative, and dotted lines zero potential. In all cases the potential maxima are well-defined and sharply peaked, mostly located close to the high sides of the ribs. On the other hand, the potential minima are broad and poorly defined, and they are located on terrace-like positions away from the ribs. In the case of Figure 5b the potential minima are close to kink-type positions. Besides contours of the electric field magnitude shown in Figure 5c,

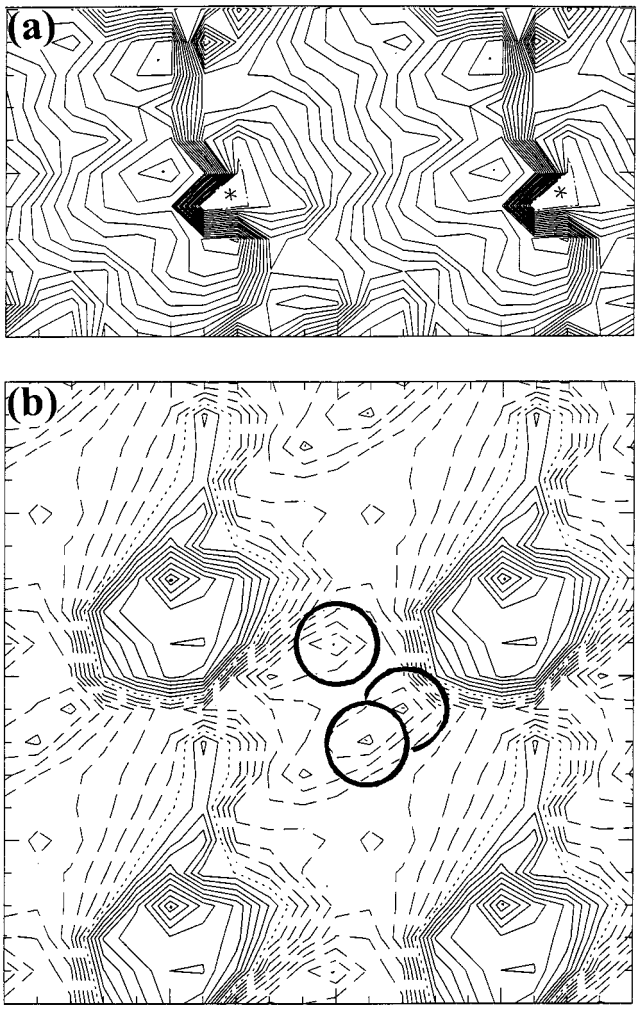

Figure 3. Surface maps of the KDP prism with reference to a fluid particle with VDW radius 0.8 Å. (a) Area ~7.8 × 3.9 Å of 2 × 1 primitive unit cells || (100). Height contours of undulated surface of closest approach between the VDW spheres of the ions on the KDP prism and the reference particle with $r_{VDW} = 0.8$ Å. Asterisks mark the local minimum height locations. (b) Area ~7.8 × 7.8 Å of ~2 × 2 primitive unit cells || (100). Equipotential curves at locations accessible to fluid particles of 0.8 Å, using as input the grid points of the surface in (a), where solid, dotted, and dashed lines indicate positive, zero, and negative potential, respectively. Three possible adsorption sites at local minima of a cation with radius 0.80 Å, not to scale.

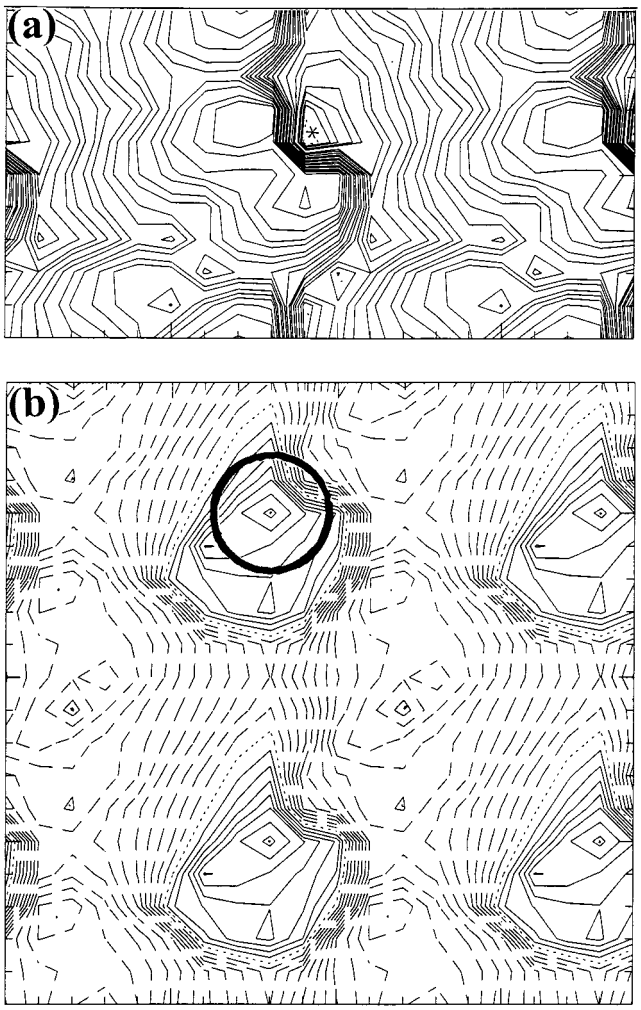

Figure 4. Surface maps of the KDP prism with reference to a fluid particle with VDW radius 2.0 Å. (a) Area ~7.8 × 3.9 Å of 2 × 1 primitive unit cells || (100). Height contours of undulated surface of closest approach between the VDW spheres of the ions on the KDP prism and a particle with $r_{VDW} = 2.0$ Å. Asterisks mark the local minimum height locations. (b) Area ~7.8 × 7.8 Å of ~2 × 2 primitive unit cells || (100). Equipotential curves at locations accessible to fluid particles of 2.0 Å, using as input the grid points of the surface in (a), where solid, dotted, and dashed lines indicate positive, zero, and negative potential, respectively. Possible adsorption site of an anion with radius 2.0 Å, not to scale.

contours of the direction (normal or tangential) of the electric field vector are possible projected on the plane. Zero field is indicated by dotted lines. The field maxima are sharply defined and located away from the ribs at terrace-like positions.

Adsorption sites are heuristically shown. The van der Waals radius 0.8 Å used in Figure 3a is indicative of a cation; Figure 3b shows possible adsorption sites at local potential minima. The van der Waals radius 2.0 Å used in Figure 4a is indicative of an anion; Figure 4b shows a possible adsorption site at a local potential maximum. The van der Waals radius 1.4 Å used in Figure 5a could be indicative of either a cation or an anion and is also equal to the radius of a water molecule. Figure 5b shows adsorption sites of an anion at a local potential minimum and cations at local potential maxima. Figure 5c shows the adsorption site of a water molecule at a local field maximum.

5. Summary and Conclusions

Criteria promoting a correct interpretation of surface X-ray diffraction data, and subsequently the effect of the solvent on the surface structure and growth morphology of ionic compounds, are summarized below.

(a) Completeness of the Employed Set of Theoretically Valid Trial Solutions. X-ray diffraction data processing relies on selecting, by means of trial and error out of a set of input alternatives, the configuration which gives the best fit with the experimental outcome. The trial solutions consist of combinations of a "surface cell" and a "bulk cell", corresponding, respectively, to the topmost and subsequently stacked growth layers with orientation (*hkl*). The layers are generated by applying to this cell-combination lattice translations || (*hkl*). In the absence of surface reconstruction or relaxation, the bulk and surface trial cells are indistinguishable.

The set of valid trial solutions consists of F slices as defined by the Hartman−Perdok theory[6,7] and can be computed graph-theoretically from first principles.[3−5] Because numerous trial solutions exist with identical outermost surface terminations, but radically different electrostatic surface properties, it is essential to take into account the complete set of trial solutions,

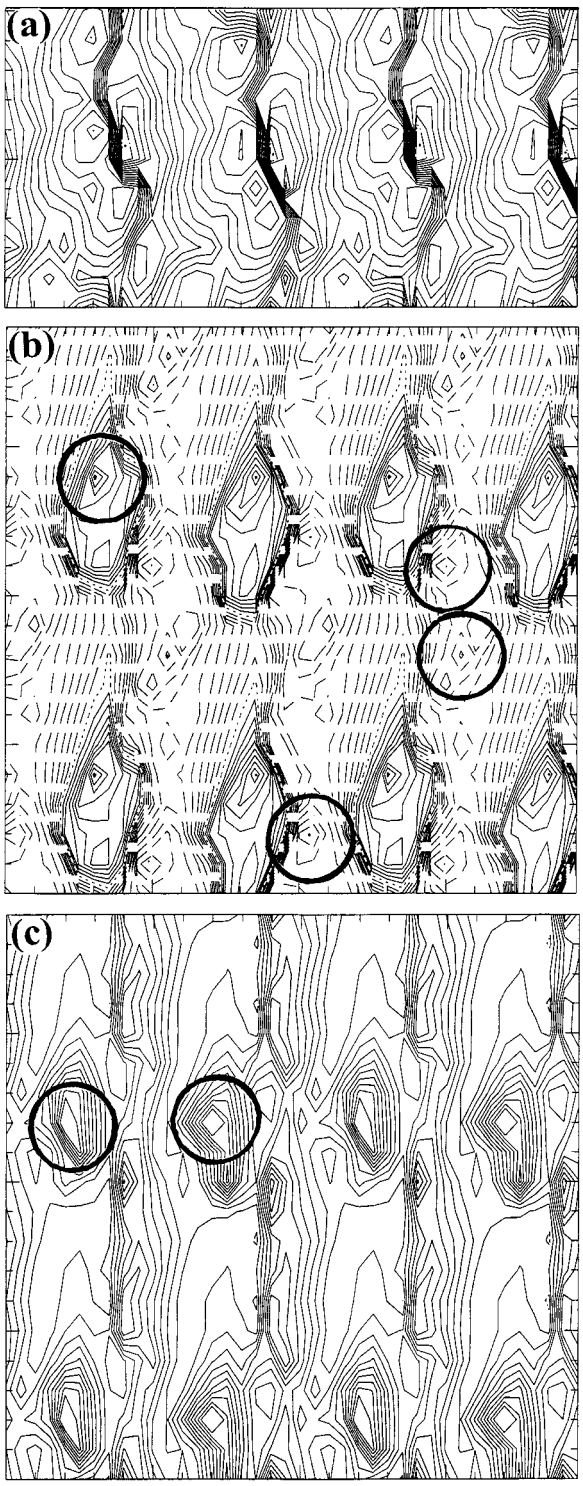

Figure 5. Surface maps of the KDP prism with reference to a fluid particle with VDW radius 1.4 Å. (a) Area ~7.8 × 3.9 Å of 2 × 1 primitive unit cells || (100). Height contours of undulated surface of closest approach between the VDW spheres of the ions on the KDP prism and a particle with $r_{VDW} = 1.4$ Å. Points mark local minimum height locations. (b) and (c) Area ~7.8 × 7.8 Å of ~2 × 2 on primitive unit cells || (100). (b) Equipotential curves at locations accessible to fluid particles of 1.4 Å, using as input the grid points of the surface in (a), where solid, dotted, and dashed lines indicate positive, zero, and negative potential, respectively. Possible adsorption sites: on the left, at a local maximum of an anion of radius 1.4 Å; on the right, at three local minima of cations of radius 1.4 Å, not to scale. (c) Contours of the electric field magnitude at locations accessible to fluid particles of 1.4 Å, using as input the grid points of the surface in (a). Two possible adsorption sites of a water molecule of 1.4 Å, not to scale.

and at the very least, that subclass of trial solutions that exhibit identical surface terminations as the solution associated with the best fit.

(b) Maintaining the Integrity of the Chemical Composition of the Growth Layer. Misinterpretations and self-contradictions arise when attention is restricted to the charge distribution at the surface boundary, while ignoring the remaining composition and step height of the growth layer.[2] All electrostatic quantities including surface polarity are determined by the charge composition of the entire trial layer as generated by the entire trial cell. The mere instance that at the surface termination geometrical planes of charges of one sign follow planes of charges of the opposite sign is neither a necessary nor a sufficient condition for establishing surface polarity.

(c) Exactness in the Treatment of the Electrostatic Surface Properties. It is well-known that the behavior of charged or polar particles in the near-surface liquid, and in consequence their effect on crystal morphology, depends on the electrostatic properties of the adjacent surface. In turn, the role of these liquid particles can only be assessed by including in the calculation the charge distribution within the entire growth layer as well as the (practically infinite) stacking of such layers forming the physical specimen used in the experiment.

In the case under study, KDP grows out of an aqueous solution, sometimes including metal impurities. The particles adjacent to the growth front are polar water molecules and ions. The surface−water interaction is dictated by the surface distribution of the electric field and the surface−ion interaction by the surface distribution of the potential.

Ewald surface maps of the potential and field distributions at surfaces of closest approach between the van der Waals spheres of structure particles and particles of the interfacial fluid provide a faithful representation of the fine-scale adsorption behavior of ionic and polar species in near-surface liquid. The maintained exactness and independence from adjustable parameters allow one to model arbitrarily specified bulk-cell and surface-cell configurations serving as trial solutions. The reported tool for a theoretical interpretation of surface X-ray diffraction results has general applicability to structures with Coulomb dominance and complex surface configurations, in the presence or absence of relaxation or reconstruction. Detailed expressions for the site electrostatic potential and site electric field vector are found in ref 17.

Acknowledgment. Co-author of ref 2, P. Bennema of the Department of Solid State Chemistry, University of Nijmegen, is acknowledged for clarifying his contribution on surface electrostatics to the work of ref 2. Members of that department are acknowledged for discussions. Thanks are due to the Netherlands Foundation for Research in Astronomy (ASTRON) for use of graphics facilities.

Appendix. Spatial Distribution of Solvent-Accessible Surface Locations

The site potential and electric field due to a semi-infinite crystal specified according to a given bulk cell and surface cell are calculated on an undulated surface of closest approach between the van der Waals radii of the crystal and of the given fluid species. The (*hkl*) face is taken as the $a-b$ plane. The surface is delimited by the van der Waals spheres of the particles of the solid, with radii ρ_i and mass centers at $\vec{r}_i = (x_i, y_i, z_i)$. A two-dimensional grid of points is constructed by the locations of closest approach between the van der Waals (VDW) spheres of the fluid particles and the van der Waals spheres at the solid

surface. The axial fractional coordinates of the grid on *a* and *b* comprise a set of equally spaced points $\{(X, Y)\}$. $\{G\}$ denotes a collection of discrete grid lines. A discrete set of coordinates *Z* on the *c* axis is associated with each discrete point (*X*, *Y*) on the *ab* plane. When *Z* is allowed to vary, it traces a grid line *G* parallel to *c*. As will be seen below, *Z* depends on the properties of the solid particles and is characterized by the value of the VDW radius of the fluid particle species.

A fluid particle with VDW radius ρ_F may assume a position vector $\vec{R}_F = (X, Y, Z)$ on any grid line *G*, provided its VDW sphere does not overlap with the VDW sphere of any solid particle *i*. Therefore, the allowed values of *Z* for a given grid line *G* satisfy $|\vec{R}_F - \vec{r}_i| \geq \rho_F + \rho_i$ for all *i*. This is alternatively expressed in terms of the polynomial $P(Z)$:

$$P(Z) = |\vec{R}_F - \vec{r}_i|^2 - (\rho_F - \rho_i)^2 \equiv c^2(Z - Z^G_{+i})(Z - Z^G_{-i}) \geq 0 \quad (1)$$

$$Z^G_{\pm i} = z_i - \frac{\vec{g}_i \cdot \vec{c}}{c^2} \pm \frac{\sqrt{D^G_i}}{c^2}$$

$$\vec{g}_i \equiv (X - x_i)\vec{a} + (Y - y_i)\vec{b}$$

$$D^G_i \equiv (\vec{g}_i \cdot \vec{c})^2 - g_i^2 c^2 + (\rho_F + \rho_i)^2 c^2$$

where *X* and *Y* belong to a discrete set of grid points. $P(z) = 0$ when $D^G_i = 0$, indicating one contact point between solid particle *i* and fluid particle *F*. When $D^G_i = 0$ *for all* solid particles *i*, the coordinate *Z* is free to assume any value. The unphysical complex roots with $D^G_i < 0$ impose no restrictions on *Z*. When $D^G_i > 0$, the allowed values of *Z* correspond to $P(Z) > 0$, giving $Z \leq Z^G_{-i}$ or $Z \geq Z^G_{+i}$. Locations of the fluid particle with *Z* values in the interval of overlap of sphere ρ_F and any of the spheres ρ_i are inadmissible. Therefore, the admissible locations, $\vec{R}_F$, of the fluid spherical particle with VDW radius ρ_F on grid line *G* are given by

$$\vec{R}_F = (X, Y, Z)$$

$$Z^G_{-i} \leq Z \leq Z^G_{+i}, \qquad \text{for all } i \quad (2)$$

The net restriction imposed on Z^G implies that the admissible values of *Z* take one of two forms: first, *Z* values in the intervals

$$Z^G_{+j} \leq Z \leq Z^G_{-k} \quad (3)$$

with $j \neq k$ are locations in gaps in the bulk. The second group consists of *Z* values satisfying

$$\max\{Z^G_i;\, i \in \text{solid}\} \leq Z \quad (4)$$

The equality sign implies a unique position of closest approach between the fluid particle and solid surface along the line *G*,

$$\max\{Z^G_i;\, i \in \text{solid}\} \leq Z^G_0 \quad (5)$$

It should be emphasized that in eqs 1−5 the indices *i*, *j*, and *k* enumerate particles in the solid. The classification of the locations accessible to the fluid particles into "bulk-gap" positions on the one hand and "surface closest-approach" positions on the other refers to each individual grid line. Hence, taken over all grid lines collectively, some so-called surface locations could happen to lie below bulk-gap locations, especially in heavily corrugated surface boundaries.

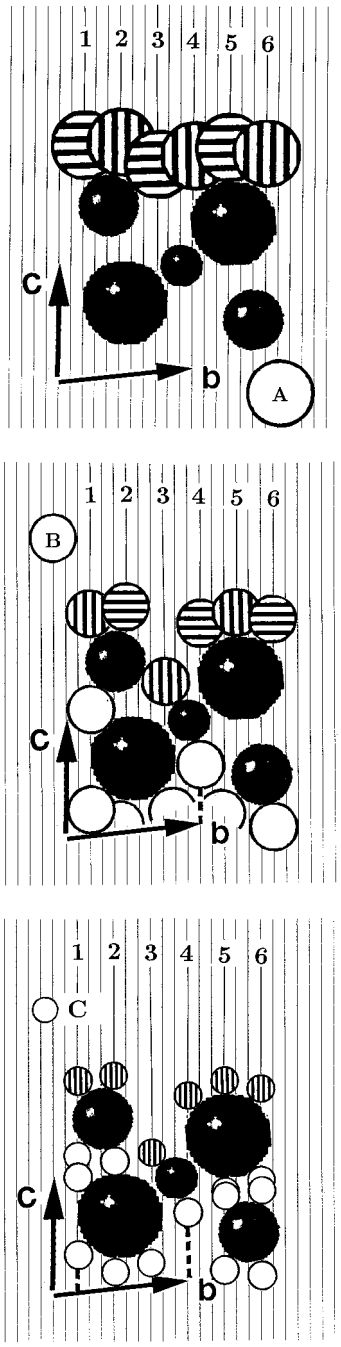

Figure 6. Illustration of accessible locations of VDW spheres of fluid particles with respect to the VDW spheres of solid particles on the (001) surface. Only one unit cell of the solid structure is shown projected on (100). Solid circles are particles belonging to the structure, immersed in an imaginary collection of grid lines $\{G\}$ with equally spaced fractional axial coordinates. Accessible positions for fluid particles of three different VDW radii (A−C) are shown for a selection of grid lines 1−6, highlighted with boldface line types. Bulk-gap positions are denoted by open circles. Overlapping circles or boldface dashed lines indicate a range of positions as in eq 3. Closest-approach surface positions are denoted by striped circles, eq 4.

The locations accessible to VDW spheres of fluid particles is schematically depicted in Figure 6. The extent of the solid is taken simply as a block of $1 \times 1 \times 1$ unit cells with four formula units and with surface orientation (001). The possible solutions for the *Z* coordinate are shown for a selection of six grid lines and for three different VDW radii of fluid particles, $\rho_A > \rho_B >$

ρ_C. The distinction between bulk-gap solutions in the range of relation (3) and surface closest-approach positions, eq 4, is clearly visible. The output on bulk-gap locations is ignored for the present purposes. The spatial distribution comprising the grid points with Z coordinates given by eq 5 serve as input for the ionic surface maps.

References and Notes

(1) Hartman, P. *Acta Crystallogr.* **1956**, *9*, 721.

(2) De Vries, S. A.; Goedtkind, P.; Bennett, S. L.; Huisman, W. J.; Zwanenburg, M. J.; Smilgies, D.-M.; De Yoreo, J. J.; Van Enckevort, W. J. P.; Bennema, P.; Vlieg, E. *Phys. Rev. Lett.* **1998**, *80*, 2229.

(3) Strom, C. S. *Z. Kristallogr.* **1980**, *153*, 99.

(4) Strom, C. S. *Z. Kristallogr.* **1981**, *154*, 31.

(5) Strom, C. S. *Z. Kristallogr.* **1985**, *172*, 11.

(6) Hartman, P. *Acta Crystallogr.* **1958**, *11*, 365, 459; In *Crystal Growth: An Introduction*; Hartman, P., Ed.; North-Holland: Amsterdam, 1973; p 367; The dependence of crystal morphology on crystal structure. In *Growth of Crystals*, Sheftal, N. N. Ed.; Consultants Bureau: New York, 1969; Vol. 7, pp 3−18.

(7) Strom, C. S.; Grimbergen, R. F. P.; Bennema, P.; Meekes, H.; Verheijen, M. A.; Vogels, L. J. P.; Wang, M. Ionic Crystals in the Hartman-Perdok Theory with Case Studies. In *Molecular Modeling Applications in Crystallization*; Myerson, A. S., Ed.; Cambridge University Press: New York, 1999; pp 228−312, and references therein.

(8) Berkowits-Yellin, M. *J. Am Chem. Soc.* **1985**, *107*, 8239.

(9) Van der Voort, E.; Hartman, P. *J. Cryst. Growth* **1988**, *89*, 603.

(10) Strom, C. S.; Vogels, L. J. P.; Verheijen, M. A. *J. Cryst. Growth* **1995**, *155*, 144.

(11) The bonds f, g, h and the hydrogen bonds in Figures 1 and 2 are defined in refs 10 and 7 as follows (with $P \equiv H_2PO_4^-$ and $K \equiv K^+$): f-bonds: $P(0,0,0)-K(0,0,0.5)$. g-bonds: $P(0,0,0)-K(0,0.5,0.25)$, and $P(0.5,0,0.25)-K(0,0,0.5)$. h-bonds: $P(0,0,0)-K(0.5,0.5,0)$. hydrogen bonds: $P(0,0,0)-P(0.5,0,0.25)$.

(12) Alexandru, H. V. *Cryst. Res. Technol.* **1995**, *30*, 1071.

(13) Van der Voort, E.; Hartman, P. *J. Cryst. Growth* **1990**, *106*, 622.

(14) The authors of ref 2 might have been alerted to the above fundamental inconsistency if their determination of the theoretical growth layers was sufficiently adequate to include, e.g., layers of the type of Figure 2C. The commercial software used by them, Cerius2 supplied by MSI in Cambridge, includes an inadequate imitation of the graph-theoretical software of ref 5, failing to compute growth layers with irreducible borders.

(15) Van der Voort, E.; Hartman, P. *J. Cryst. Growth* **1990**, *140*, 450.

(16) Heyes, D. M. *Phys. Chem. Solids* **1980**, *41*, 281; *J. Chem. Phys.* **1981**, *74*, 1924.

(17) Strom, C. S.; Hartman, P. *Acta Crystallogr. A* **1989**, *45*, 371, program *SURFPOT*.

(18) Ewald, P. P. *Ann. Phys. (Leipzig)* **1921**, *64*, 253.

(19) Strom, C. S. *Program SURFGRID* composed of *SURFPOT modules*, **1997**.